ADVANCED MATERIALS
www.advmat.de

Topology Optimized Architectures with Programmable Poisson's Ratio over Large Deformations

Anders Clausen, Fengwen Wang, Jakob S. Jensen, Ole Sigmund, and Jennifer A. Lewis**

Structural materials are used in myriad applications, including aerospace, automotive, biomedical, and acoustics. Most materials have positive or zero Poisson's ratio, with cork serving as a well-known example of the latter type of behavior. The Poisson's ratio describes the relative amount a given material contracts transversally when axially stretched. Recently, artificial materials that exhibit a negative Poisson's ratio have been introduced.[1–3] These auxetic materials expand transversally when axially stretched, seemingly defying the fundamental laws of nature.[1–3] They exhibit enhanced mechanical properties, such as shear resistance,[4,5] indentation resistance,[6–9] and extraordinary damping properties,[10] making them well suited for targeted applications. To date, several types of auxetic materials have been introduced.[2,3,11–20] However, most current embodiments suffer from two primary limitations: i) they only exhibit the desired response over a narrow range of strains (less than a few percent) and ii) they are difficult to manufacture in a scalable manner.[17,21–25] While recent structures (e.g., chiral honeycombs,[14] tilting square structures,[24] or Bucklicrystals[19]), for specific values of Poisson's ratio, exhibit near constant values over large strains, they are either not generalizable to other Poisson's ratio values or they exhibit low effective stiffness and/or must be pre-stressed to yield the desired performance.

Here, we combine topology optimization to programmably design their architecture with 3D printing to digitally fabricate the designs and validate against the numerically predicted behavior. Specifically, we create a new class of architected materials with programmable Poisson's ratios between –0.8 and 0.8 that display a nearly constant Poisson's ratio over large deformations of up to 20% or more. **Figure 1** shows two representative examples of microstructures designed using topology optimization.[26] The linear model that is applied by existing design methods (Figure 1a) assumes small deformations. By contrast, an emerging approach (Figure 1b), described in detail in a recent study[26] by Sigmund and co-workers, uses a geometrically non-linear model and includes a requirement of a constant prescribed Poisson's ratio when straining the material. While both examples are designed to have a Poisson's ratio of –0.8, the performance of the linearly designed material rapidly deteriorates when the material is strained more than a few percent (Figure 1c).

Mathematically, the optimization goal is defined as minimizing the error between the actual and the pre-defined value of Poisson's ratio over a range of discrete, nominal strain values up to 20%.[26] To ensure scalable fabrication of these architectures, several geometric constraints are imposed on the topology optimization design problem. A requirement of uniform structural features is implemented as a combination of imposing a minimum[27,28] and a maximum length scale. The topology optimization step leads to a beam-like layout, which may be converted into a simplified design composed of a set of parameterized superellipses. Uniform feature size is guaranteed by specifying a constant width for all the superellipses, while the length of each superellipse is controlled by design points (Figure S1, Supporting Information). Using shape optimization to fine-tune the superellipse designs, we obtain architectures with uniform features having the desired response.

To demonstrate our approach, nine reference architectures are designed with equally dispersed and strain-independent constant Poisson's ratio values between –0.8 and 0.8. Based on this discrete set of architectures, we derive a simple generic parameterization that provides a design guideline for any targeted value of the Poisson's ratio within the range of –0.8 to 0.8. The details of the topology and shape optimization methodology as well as the derivation of the generic parameterization are provided in the Supporting Information and illustrated in Figure S2. We use direct ink writing (DIW),[29–31] an extrusion-based 3D printing method, to fabricate these topologically optimized materials (**Figure 2**a). Inspired by initial results from the topology optimization process, we realized that materials with a negative or zero Poisson's ratio could be designed to ensure a continuous print path (Figure 2b), which is not generally obtained in topology optimized architectures. This ultimately ensures their scalable fabrication via multinozzle arrays.[32] The uniform feature size obtained with the superellipse approach allows printing with a constant nozzle speed and volumetric flow, thereby minimizing patterning errors. The structures with a strictly positive Poisson's ratio have a different topology requiring a modified printing strategy. The unit cell consists of round features connected by straight members (Figure 2c) and may be fabricated with a continuous print path

A. Clausen, Dr. F. Wang, Prof. O. Sigmund
Department of Mechanical Engineering
Solid Mechanics
Technical University of Denmark
2800 Kongens Lyngby, Denmark
E-mail: sigmund@mek.dtu.dk
Prof. J. S. Jensen
Department of Electrical Engineering
Centre for Acoustic-Mechanical Micro Systems
Technical University of Denmark
2800 Kongens Lyngby, Denmark
Prof. J. A. Lewis
School of Engineering and Applied Sciences
Wyss Institute for Biologically Inspired Engineering
Harvard University
Cambridge, MA 02138, USA
E-mail: jalewis@seas.harvard.edu

DOI: 10.1002/adma.201502485

© 2015 WILEY-VCH Verlag GmbH & Co. KGaA, Weinheim

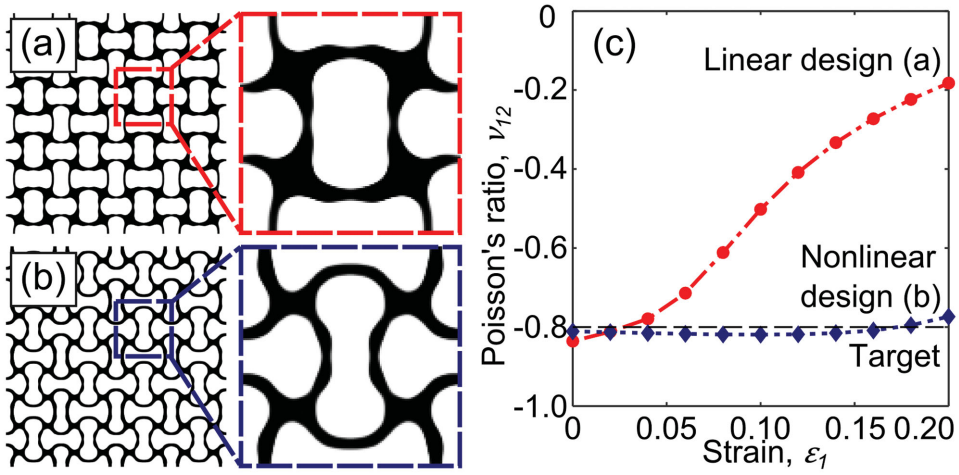

Figure 1. Topology optimized microstructures for auxetic materials via a) linear and b) geometrical non-linear modeling. c) Dependency on strain of the Poisson's ratio for large deformations for the respective materials.

by printing the connecting features with two passages of the nozzle, as indicated by the arrow in Figure 2c. This approach translates into a requirement of piecewise uniform feature size, with the double-printed features having correspondingly larger width, which is easily fulfilled using the superellipse approach.

We fabricated a complete series of topology optimized architectures that exhibit nearly constant values of Poisson's ratio over large deformations across nine equally dispersed values ranging between –0.8 and 0.8 (**Figure 3**a–c). These samples (ten layers) are printed using a silicone-based elastomeric ink and then cured (see, for example, Movie S1, Supporting Information). Each sample is then subjected to uniaxial tensile testing (Figure 3e) and its performance is compared to the numerical prediction (Figure 3f). The deformation patterns for samples of the two extremal Poisson's ratio values (–0.8 and 0.8) clearly demonstrate the large deformations associated with the expanding (Movie S2, Supporting Information) versus contracting behavior (Figure 3d,g). The definition of Poisson's ratio used for design and validation is the negative ratio of the transverse strain, ε_2, to the longitudinal strain, ε_1

$$\nu = \frac{-\varepsilon_2}{\varepsilon_1} \tag{1}$$

The applied strain measure is the engineering strain, i.e., $\varepsilon = \Delta L / L_0$, where ΔL is the change in distance between two points initially separated by the distance L_0. The experimentally measured values are an average over the four (two by two) central unit cells. Despite minor deviations, the experimental results are in good agreement with the predicted behavior for both the negative and positive Poisson's ratio designs. In the latter case, the experimental values are slightly below the numerical curve for large strains in all samples. This deviation likely arises to slight geometrical differences between the fabricated samples and the programmed designs, rather than flaws in the numerical model. For example, the initial (lower) layers deform slightly due to gravitational and viscous forces as subsequent (upper) layers are printed. The upper layers are drawn slightly inwards at sections with strong curvature due to viscous forces in the ink. Hence, the desired uniform feature size is not perfectly realized in those samples.

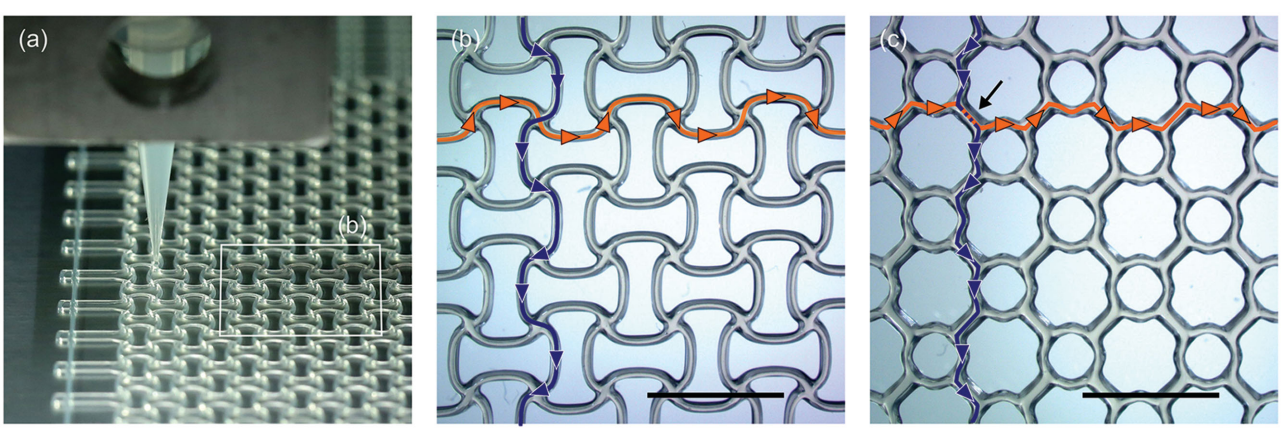

Figure 2. 3D printing method and constraints. a) Optical image of the fabrication of PDMS-based architectures using direct ink writing. b) Print path (indicated by superposed solid lines with triangle markers) for these structures for negative and zero Poisson's ratio. c) Print path for positive Poisson's ratio. For segments with overlapping print paths (indicated by arrow), the features are correspondingly wider. The scale bars in (b) and (c) are 5 mm.

© 2015 WILEY-VCH Verlag GmbH & Co. KGaA, Weinheim

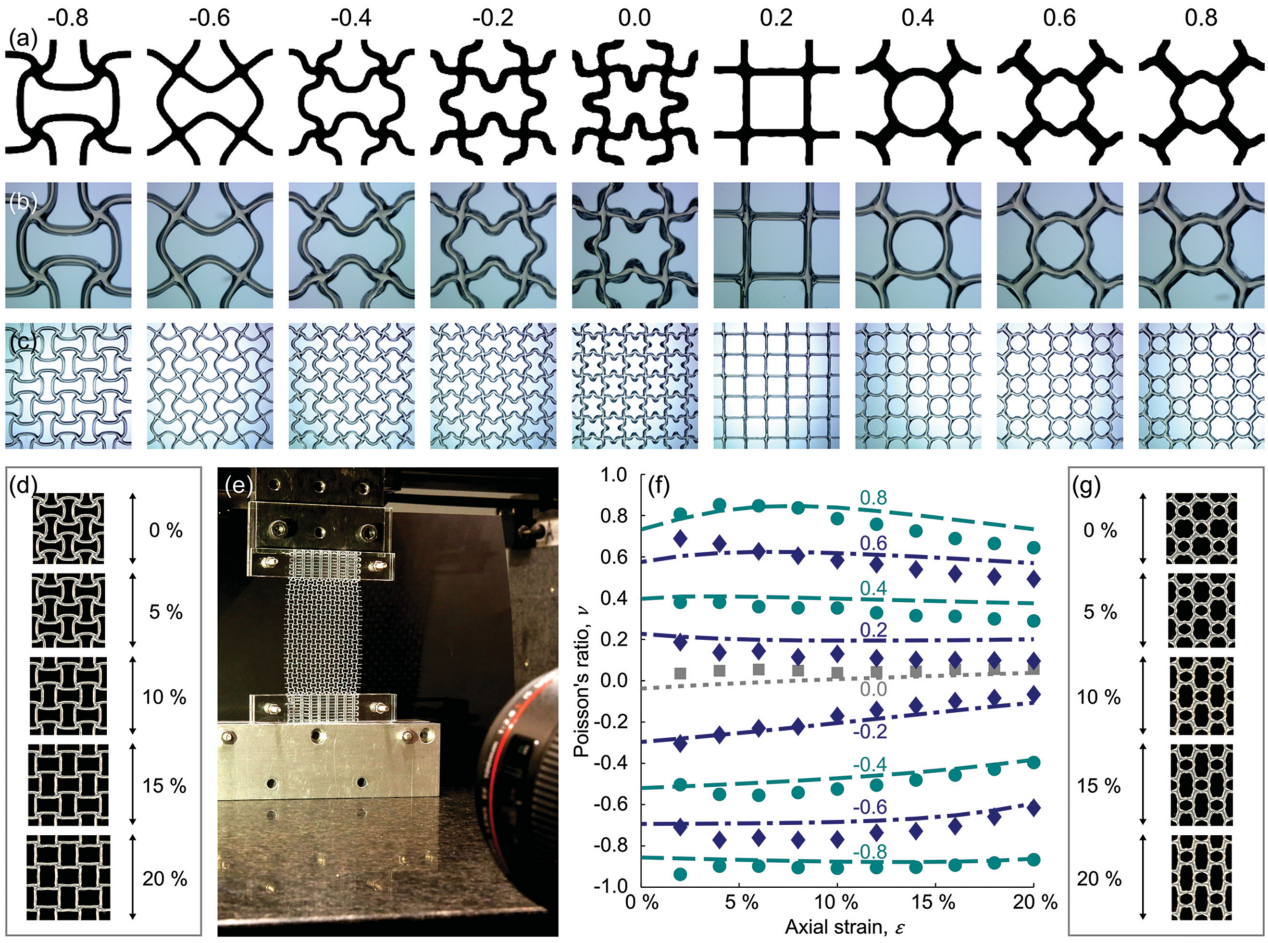

Figure 3. Topology and shape optimized architectures. a) Designed and b) printed unit cells for a programmable range of Poisson's ratio values. c) 3 × 3 unit cells of the corresponding PDMS-based architectures. d) Deformation pattern of the 2 × 2 central unit cells corresponding to given longitudinal nominal strain values for $\nu = -0.8$ (in (g) for $\nu = 0.8$). e) Experimental setup for tensile tests. f) Comparison between experimental (points) and numerically predicted (dashed lines) results. Unit cell size for all architectures in (a)–(g) is 5 mm.

As noted earlier, the four optimized microstructures with positive Poisson's ratio share a very similar generic configuration (**Figure 4**a), while the five optimized microstructures with negative or zero Poisson's ratio share another (albeit related) generic configuration (Figure 4b). To clearly demonstrate their configuration evolution versus Poisson's ratio only the skeletons of the optimized materials are shown. Based on the optimized design points for the nine reference designs, the microstructural configuration for any given Poisson's ratio within the interval [–0.8, 0.8] can be obtained by using a B-spline interpolation of the design points. The validity of this interpolation is illustrated in Figure 4c, where the total absolute performance

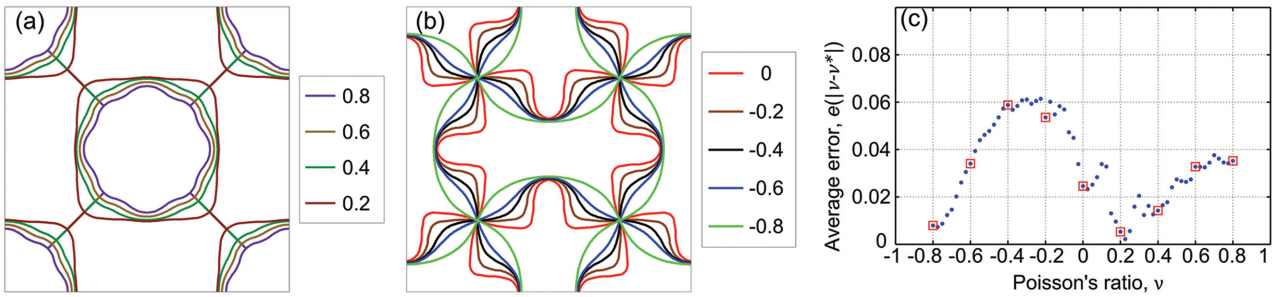

Figure 4. Generic parameterization of engineered architectures. Visual comparison of the unit cell layout for a) positive and b) negative or zero Poisson's ratio. c) Average absolute error for parameterized designs for any given Poisson's ratio. The red square points indicate the nine optimized reference structures.

© 2015 WILEY-VCH Verlag GmbH & Co. KGaA, Weinheim

error, averaged over the entire strain range, is displayed not only for the nine reference structures, but also for seven interpolated structures between each design point in both the positive and the negative range of Poisson's ratio. Figure 4c clearly shows that all designs perform well in a predictable fashion with only small variations.

In summary, by combining topology optimization with additive manufacturing, we have created a new class of architected materials. We have developed a simple geometric parameterization for the layout of the microstructural designs based on numerical optimization studies. We have fabricated material architectures with programmable Poisson's ratio values ranging from –0.8 to 0.8 over deformations that are an order of magnitude greater than those observed previously. Our approach opens new avenues to the design and rapid fabrication of programmable materials possessing exotic properties.

Experimental Section

Silicone Ink: The ink is a poly(dimethylsiloxane) (PDMS) silicone material, SE 1700 (Dow Corning), which consists of a 10:1:1 mix ratio of SE 1700 Clear Base, SE 1700 Catalyst (both Dow Corning) and silicone oil (viscosity 350 cSt (25 °C), Sigma–Aldrich Chemistry), respectively. The parts were mixed in a 15 mL container for 5 min at 2000 rpm using a planetary mixer (Dual Asymmetric Centrifugal SpeedMixer, FlackTek Inc., DAC 600.2 VAC-P). For each test specimen, 6 g of mixed material was prepared.

3D Printing: The ink was loaded into a 10 cc, luer-lock syringe (Nordson EFD Optimum) and centrifuged for 10 min at 3000 rpm to remove air bubbles (Thermo Electron Corporation IEC Centra CL2 Centrifuge). The loaded syringe was placed on an Aerotech 3-axis positioning stage (Aerotech, Inc.). Ink deposition was controlled pneumatically using an Ultimus V pressure box (Nordson EFD). The ink was printed through a 200 μm luer-lock syringe tip (Nordson EFD) onto a glass plate covered with PTFE-coated aluminum foil to prevent adhesion (Bytac, Saint-Gobain). Print paths were generated from optimized designs by converting node positions into parameterized G-code scripts. Test specimens (10 layers with 136 μm layer thickness) were printed on a custom-designed three-axis motion-controlled stage (Aerotech, Inc). Printed parts are cured at 100 °C for 4 h.

Uniaxial Tensile Tests: For each of the fabricated architectures, a test specimen with overall dimensions of 60 mm × 40 mm consisting of 12 (longitudinal) by 8 (transversal) unit cells (5 mm × 5 mm) was printed. At both ends, a 15 mm grid was printed to allow mounting the sample for mechanical testing. For the tensile tests, the attachment grid at both ends was friction fastened between two pieces of purpose cut 6 mm acrylic plate, the latter held together using bolts and nuts. Each sample was tested in a vertical setup. The top end was attached to the *z*-stage of the Aerotech positioning system using screws. The bottom end was attached between two steel blocks held in place by gravity. The initial sample length (distance between acrylic plates of opposite ends) was measured using a digital caliper. The sample was strained at 2% increments between 0% and 20%. Each step was monitored using a digital SLR camera (22.3 M Pixels Canon 5D Mark III with a Canon US Macro 100 mm objective) synchronized with the setup.

Image Analysis: Each photo from the strain test was converted to a contour plot using the MATLAB Image Processing Toolbox. Distances, measured in pixels between corresponding features, were tracked between images for all nominal strain values for each sample. Numerical simulations of the entire tensile test specimen revealed that boundary effects, such as constraints on both ends of the specimen, only cause minor deviations (less than 5%) when evaluating the Poisson's ratio using the four unit cells located in the center of the specimen. Hence, experimental strain values used for computing the Poisson's ratio were determined as an average over the four unit cells within the 2 × 2 array located in the center of each specimen.

Supporting Information

Supporting Information is available from the Wiley Online Library or from the author.

Acknowledgements

A.C. and F.W. contributed equally to this work. A.C. and O.S. acknowledge financial support from the Villum Foundation (the NextTop project) and DTU Mechanical Engineering. F.W. and J.S.J. acknowledge financial support from the ERC starting Grant through INNODYN. J.A.L. acknowledges support from Army Research Office Award No. W911NF-13-0489. The experimental work was carried out in relation to A.C.'s research stay at the Lewis Research Group during the Fall, 2014. The authors would like to acknowledge Joseph Muth and Dr. Jordan R. Raney from the Lewis group for valuable input on the experimental work, and Dr. Lori K. Sanders for assistance on the photographic documentation.

Received: May 24, 2015
Revised: July 13, 2015
Published online: August 20, 2015

[1] L. J. Gibson, M. F. Ashby, G. S. Schajer, C. I. Robertson, *Proc. R. Soc.* **1982**, *382*, 25.
[2] R. Lakes, *Science* **1987**, *235*, 1038.
[3] K. E. Evans, *Endeavour* **1991**, *15*, 170.
[4] J. Choi, R. Lakes, *J. Mater. Sci.* **1992**, *27*, 5375.
[5] J. Choi, R. Lakes, *J. Mater. Sci.* **1992**, *27*, 4678.
[6] R. Lakes, K. Elms, *J. Compos. Mater.* **1993**, *27*, 1193.
[7] N. Chan, K. E. Evans, *J. Cell. Plast.* **1998**, *34*, 231.
[8] K. L. Alderson, A. P. Pickles, P. J. Neale, K. E. Evans, *Acta Metall. Mater.* **1994**, *42*, 2261.
[9] K. L. Alderson, A. Fitzgerald, K. E. Evans, *J. Mater. Sci.* **2000**, *35*, 4039.
[10] C. Chen, R. Lakes, *J. Eng. Mater. Technol.* **1996**, *118*, 285.
[11] E. Friis, R. Lakes, J. Park, *J. Mater. Sci.* **1988**, *23*, 4406.
[12] K. L. Alderson, K. E. Evans, *Polymer* **1992**, *33*, 4435.
[13] G. W. Milton, *J. Mech. Phys. Solids* **1992**, *40*, 1105.
[14] D. Prall, R. Lakes, *Int. J. Mech. Sci.* **1997**, *39*, 305.
[15] R. Lakes, R. Witt, *Int. J. Mech. Eng. Educ.* **2002**, *30*, 50.
[16] T. Bückmann, N. Stenger, M. Kadic, J. Kaschke, A. Frölich, T. Kennerknecht, C. Eberl, M. Thiel, M. Wegener, *Adv. Mater.* **2012**, *24*, 2710.
[17] U. D. Larsen, O. Sigmund, S. Bouwstra, *J. Microelectromech. Syst.* **1997**, *6*, 99.
[18] K. Bertoldi, P. M. Reis, S. Willshaw, T. Mullin, *Adv. Mater.* **2010**, *22*, 361.
[19] S. Babaee, J. Shim, J. C. Weaver, E. R. Chen, N. Patel, K. Bertoldi, *Adv. Mater.* **2013**, *25*, 5044.
[20] T. Bückmann, R. Schittny, M. Thiel, M. Kadic, G. W. Milton, M. Wegener, *New J. Phys.* **2014**, *16*, 033032.
[21] O. Sigmund, *Int. J. Solids Struct.* **1994**, *31*, 2313.
[22] E. Andreassen, J. S. Jensen, *Struct. Multidiscip. Optim.* **2013**, *49*, 695.
[23] O. Sigmund, S. Torquato, I. A. Aksay, *J. Mater. Res.* **2011**, *13*, 1038.
[24] O. Sigmund, *Mech. Mater.* **1995**, *20*, 351.

© 2015 WILEY-VCH Verlag GmbH & Co. KGaA, Weinheim

[25] E. Andreassen, B. S. Lazarov, O. Sigmund, *Mech. Mater.* **2014**, *69*, 1.
[26] F. Wang, O. Sigmund, J. S. Jensen, *J. Mech. Phys. Solids* **2014**, *69*, 156.
[27] F. Wang, B. S. Lazarov, O. Sigmund, *Struct. Multidiscip. Optim.* **2011**, *43*, 767.
[28] M. Zhou, B. S. Lazarov, F. Wang, O. Sigmund, *Comput. Methods Appl. Mech. Eng.* **2015**, *293*, 266.
[29] J. E. Smay, J. CesaranoIII, J. A. Lewis, *Langmuir* **2002**, *18*, 5429.
[30] G. M. Gratson, M. Xu, J. A. Lewis, *Nature* **2004**, *428*, 386.
[31] B. Y. Ahn, E. B. Duoss, M. J. Motala, X. Guo, S.-I. Park, Y. Xiong, J. Yoon, R. G. Nuzzo, J. A. Rogers, J. A. Lewis, *Science* **2009**, *323*, 1590.
[32] C. J. Hansen, R. Saksena, D. B. Kolesky, J. J. Vericella, S. J. Kranz, G. P. Muldowney, K. T. Christensen, J. A. Lewis, *Adv. Mater.* **2013**, *25*, 96.

© 2015 WILEY-VCH Verlag GmbH & Co. KGaA, Weinheim